*Article*

# Seed-Assisted Growth of TiO$_2$ Nanowires by Thermal Oxidation for Chemical Gas Sensing

**Hashitha M. M. Munasinghe Arachchige [1,2,\*], Dario Zappa [1], Nicola Poli [1], Nanda Gunawardhana [2], Nuwan H. Attanayake [3] and Elisabetta Comini [1]**

[1]    SENSOR Laboratory, University of Brescia, Via D. Valotti 9, 25133 Brescia, Italy; dario.zappa@unibs.it (D.Z.); nicola.poli@unibs.it (N.P.); elisabetta.comini@unibs.it (E.C.)

[2]    Centre for Research and International Relations, Sri Lanka Technological Campus, Padukka 10500, Sri Lanka; nandag@sltc.ac.lk

[3]    Department of Chemistry, Temple University, 1901 North 13th Street, Philadelphia, PA 19122, USA; tuf74035@temple.edu

\*    Correspondence: h.munasinghearac@unibs.it

check for updates

**Abstract:** Herein, we report the catalyst assisted growth of TiO$_2$ one-dimensional (1D) nanowires (NWs) on alumina substrates by the thermal oxidation technique. RF magnetron sputtering was used to deposit a thin Ti metallic layer on the alumina substrate, followed by an Au catalytic layer on the Ti metallic one. Thermal oxidation was carried out in an oxygen deficient environment. The optimal thermal growth temperature was 700 °C, in a mixture environment composed by Ar and O$_2$. As a comparison, Ti films were also oxidized without the presence of the Au catalyst. However, without the Au catalyst, no growth of nanowires was observed. Furthermore, the effect of the oxidation temperature and the film thickness were also investigated. SEM, TEM, and EDX studies demonstrated the presence of Au nanoparticles on top of the NWs, indicating that the Au catalyst drove the growth process. Raman spectroscopy revealed the Rutile crystalline phase of TiO$_2$ NWs. Gas testing measurements were carried out in the presence of a relative humidity of 40%, showing a reversible response to ethanol and H$_2$ at various concentrations. Thanks to the moderate temperature and the easiness of the process, the presented synthesis technique is suitable to grow TiO$_2$ NWs for many different applications.

**Keywords:** TiO$_2$ nanowires; seed-assisted thermal oxidation; thermal oxidation; TiO$_2$ gas sensor; metal oxide nanowires

## 1. Introduction

The field of one-dimensional (1D) nanomaterial research has witnessed a remarkable growth in its attempt to drive new technologies and improve existing ones. There has been a significant interest over the past decade in 1D nanomaterials owing to their unique physical and chemical properties. These unique properties are impelled by an enhanced surface area and surface electronic properties that can vary enormously from those of their bulk counterparts [1,2]. Among these materials, TiO$_2$ 1D nanostructures received enormous attraction in the fields of photo electrochemical water spitting [3], solar cells [4], and optical devices [5] due to their compatible band-edge positions, high resistance to photo corrosion, high photocatalytic activity, lack of toxicity, and low cost [6]. Recently, TiO$_2$ 1D nanostructures are gaining a significant interest in the detection of toxic and vapors due to the properties mentioned above [7–9]. In particular, TiO$_2$ exhibits a great potential for the fabrication of gas sensors due to its high stability at a high working temperature and low cost [10–12].

Several attempts have been made to synthetize TiO$_2$ nanowires (NWs) including vapor liquid solid (VLS) [13–16], thermal oxidation [17–20], hydrothermal [21], sol gel [12,22], pulsed laser deposition [3,23],

electrospinning [24–27], and anodization method [28]. However, wet chemical methods require further cleaning processes and the nanostructures transfer on an appropriate substrate, which increase the cost of the synthesis methods. Therefore, many studies have been conducted to optimize the growth of TiO$_2$ NWs via dry physical methods.

Generally, high-temperature physical synthesis methods lead to the production of contaminant-free high-crystalline TiO$_2$ structures in the stable rutile crystalline phase. Lee et al. [13] showed the VLS growth of TiO$_2$ nanowires by the thermal evaporation of a Ti source on the alumina substrate, thanks to the deposition of a 500 nm thick Ti buffer layer on top of the Au catalyst. In that work, Ti powder was placed at high temperature inside the furnace and heated to 1050 °C, acting as a source material. Sani et al. [15] demonstrated the VLS growth of TiO$_2$ NWs on a 50 nm thick Ti buffer layer by using mixed Ti and graphite powder as a source material to reduce the evaporation temperature of Ti. In general, the thermal evaporation processes reported in the literature always require two steps, the sputtering of a Ti buffer layer and the evaporation of Ti at high temperature [16,29–31]. These processes require a high-energy consumption and a complex setup for the nanostructures growth.

Recent studies focused on the synthesis of TiO$_2$ NWs by the thermal oxidation method. This method allows the production of TiO$_2$ NWs with a stable rutile phase [32]. The oxidation of a Ti foil in an oxygen environment has been previously studied [17,20,33], and Peng et al. [18] showed that a direct oxidation of the Ti foil was also possible in an organic atmosphere. However, all studies reported so far have been carried out by using Ti foils as a substrate, in the presence of dangerous vapors such as ethanol as an oxidation gas and using an oxidation temperature above 800 °C [34].

In this paper, we report for the first time the seed-assisted synthesis of TiO$_2$ NWs directly on the alumina substrate by thermal oxidation, starting from a thin Ti layer deposited on the substrate and using only small amounts of oxygen as oxidizing gas. Thanks to the thermal oxidation method, it is possible to avoid the transfer of nanostructures from one substrate to another. This is a great advantage with respect to wet chemical synthesis techniques: The proposed method is highly scalable for a mass production, as it could be easily implemented in industrial processes. The oxidation temperature was reduced compared to the literature, allowing the formation of TiO$_2$ NWs on the alumina substrate at only 650 °C. This high-yield method allows the growth of TiO$_2$ NWs with an average diameter of 20–40 nm, with a length of several micrometers. Furthermore, these TiO$_2$ NWs show a reversible response to ethanol and H$_2$ when integrated in chemical sensing devices.

## 2. Materials and Methods

Alumina substrates (2 × 2 mm, Kyocera, Japan, 99.9% purity) were used to deposit and grow TiO$_2$ NWs. These substrates were ultrasonically cleaned for 15 min in acetone to remove dust particles, and then dried in a synthetic air flow. A thin metallic Ti layer (50, 100, or 200 nm) was deposited by RF magnetron sputtering (75 W argon plasma, chamber pressure 5.0 mTorr, and 300 °C with a deposition time of 25, 50, or 100 min). Subsequently, a deposition of a thin Au layer was performed on the Ti surface by RF magnetron sputtering (75 W argon plasma, chamber pressure 5.0 mTorr, room temperature), resulting in an agglomeration of nanoparticles (2–5 nm) acting as seed catalysts for the nanostructures growth. Finally, samples were placed in a homemade thermal oxidation chamber and were oxidized. The internal pressure of the chamber was maintained at 10$^{-1}$ mbar during the oxidation, which was carried out in a temperature range between 600–750 °C for 2–4 h in a mixed gas flow of O$_2$ (1–20 Standard cubic centimeters per minute (SCCM)) and argon (100 SCCM). Table 1 collects all experimental parameters controlled during the synthesis process.

**Table 1.** Experimental condition tested for the synthesis of TiO$_2$ NWs.

| Parameter | Condition |
| --- | --- |
| Ti layer thickness (nm) | 50, 100, 200 |
| Oxidation temperature (°C) | 600, 650, 700, 750 |
| Oxidation time (h) | 2, 3, 4 |
| Oxygen flow (SCCM) | 1, 5, 10, 20 |
| Argon flow (SCCM) | 100 |

The surface morphology of TiO$_2$ NWs was investigated by a field emission scanning electron microscope (FE-SEM, LEO 1525, Zeiss) operating at 3–5 kV. Transmission electron microscopy (TEM) images were obtained using a JEOL JEM-1400 microscope operating at 120 kV. Raman measurements were performed using a Horiba Jobin Yvon Labram HR800 Evolution confocal Raman spectrometer with a 532 nm laser excitation, Olympus MPlan N 100× microscope objective able to focus the excitation light to ~1 μm spot, and 1800 g/mm grating providing ~2 cm$^{-1}$ spectral resolution.

After the nanostructures synthesis and characterization, chemical sensing devices were fabricated as shown in Figure 1. For the functional characterization of the sensing devices performances, we used the same alumina substrates covered by TiO$_2$ NWs as active transducers. A TiW adhesion layer and Pt interdigitated electrodes (IDE) were deposited by DC magnetron sputtering on top of TiO$_2$ NWs (75 W argon plasma, 7 SCCM argon flow, 5.0 mTorr pressure at 300 °C). The TiW adhesion layer was placed between the platinum IDE and the alumina substrate to improve the mechanical adhesion of the stacked structure.

Metal oxide interactions with target gas molecules are thermally activated. Therefore, platinum heaters were fabricated on the backside of the alumina substrate using the same conditions used for the electrodes. Finally, substrates were mounted on transistor-outline (TO-39) packages by using electro-soldered gold wires. The sensors conductometric responses were tested in a stainless steel chamber (1 L volume) located inside a climatic chamber (Angelantoni, Italy, model MTC 120) with temperature set at 20 °C. Humidified air was produced by flowing the dry air through a Drechsel bottle, held in a thermostatic bath at 25 °C. Four different sensors were mounted inside the test chamber, which is able to measure the performances of the sensors simultaneously. A fixed voltage (1 V) was applied to the sensor active films and the total gas flow was set to 200 SCCM with 40% relative humidity (RH).
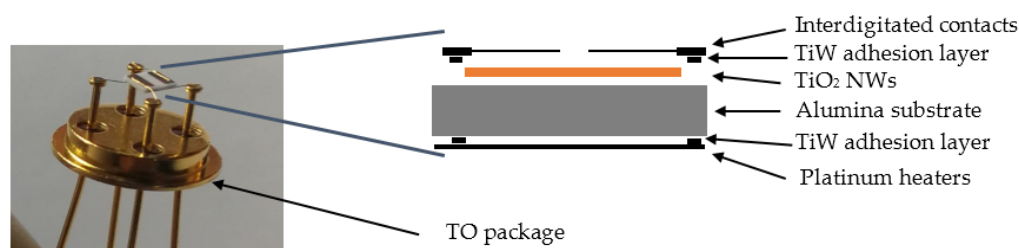


**Figure 1.** Schematic of the conductometric device fabricated.

Fabricated devices were tested towards ethanol, acetone, carbon monoxide, and hydrogen at 300, 400, and 500 °C. Prior to the introduction of the target gas, samples were stabilized for 10 h at each temperature. Sensors were exposed to the selected gas concentration for 20 min, and then the synthetic air flow was restored to recover the baseline signal. The devices response was calculated from the variation of their electrical conductance, using the following formulae for oxidizing and reducing gases, respectively.

$$Response = \frac{R_{Gas} - R_{Air}}{R_{Air}} = \frac{G_{Air} - G_{Gas}}{G_{Gas}} \tag{1}$$

$R_{Air}$ and $G_{Air}$ are the base line resistance/conductance of the sensor and $R_{Gas}$ and $G_{Gas}$ are the resistance/conductance of the sensor in the presence of the target gas.

## 3. Results

### 3.1. Morphological and Structural Characterization

As pointed out in the previous section, $TiO_2$ NWs were grown on the alumina substrate by thermal oxidation in an oxygen deficient environment. Figure 2 illustrates the SEM and TEM images of Ti (200 nm thickness) samples, grown at 700 °C with 10 SCCM oxygen and 100 SCCM argon flow for 3 h. Figure 2a shows the pure Ti metal growth at 700 °C in the mixture of $Ar/O_2$. Many dense polycrystalline grains were formed during the oxidation of the Ti metal, but these polycrystalline grains did not show any uniform orientation in the growth direction. Figure 2b shows the SEM plain-view images of the Au/Ti growth at similar conditions. The results indicate that the Au layer has a strong influence on the NWs growth, confirming that the growth of $TiO_2$ NWs is driven by Au nanoparticles (NPs) [35]. Further investigations reveal that these NWs have two dominant segments (Figure 2c). These segments of the NWs are composed of a narrow needle-like top and wide grain at the bottom.

Figure 2d shows the TEM image of some $TiO_2$ NWs, removed from the alumina substrate and dispersed on a carbon grid. TEM images clearly illustrate the presence of Au nanoparticles on top of the NWs, further confirming that Au nanoparticles have a fundamental effect on the NWs growth. NWs exhibit a quite uniform diameter and have a neck-like narrow-end close to the Au nanoparticles. Figure 3 reports the diameter distribution of the $TiO_2$ NWs. The average diameter of $TiO_2$ NWs was 20–40 nm while the length was several micrometers. In the end, this growth method resulted in being scalable and reproducible.
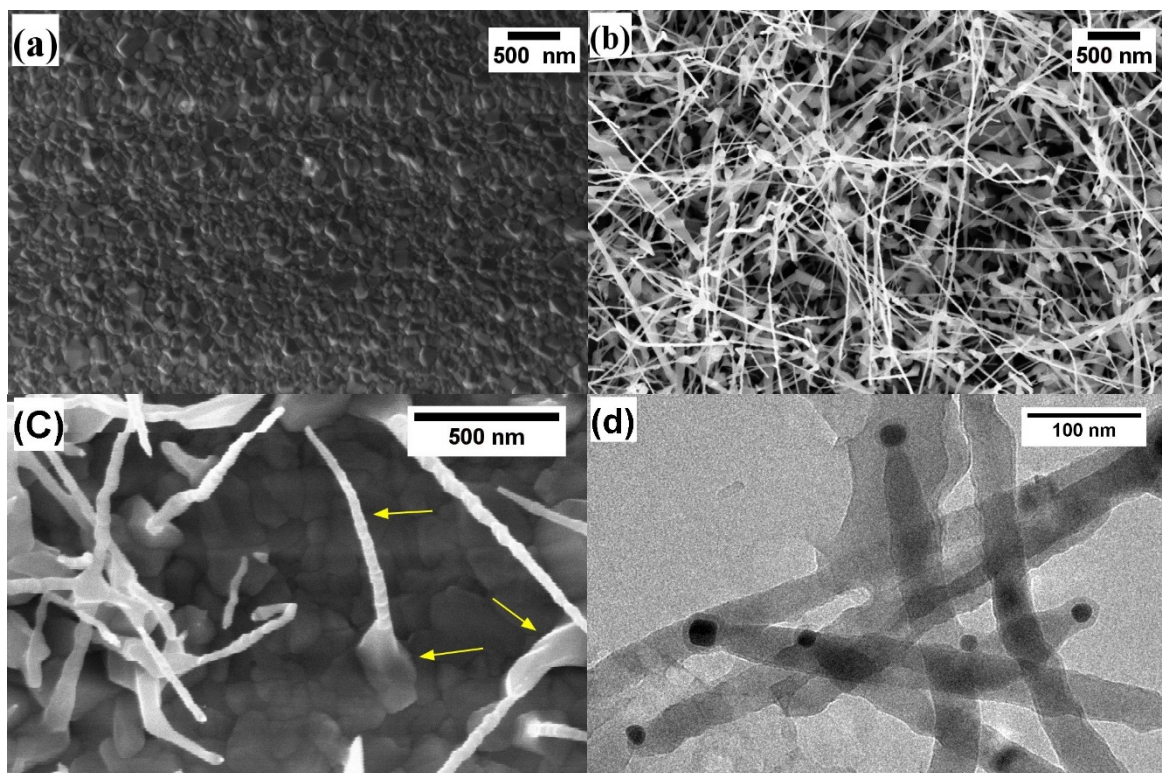


**Figure 2.** SEM plain views of $TiO_2$ nanowires (NWs) growth at 700 °C with 10 SCCM oxygen and 100 SCCM argon flow for 3 h, (**a**) without gold catalyst and (**b**) with gold catalyst. (**c**) $TiO_2$ NWs with narrow needle-like top and wide grains at the bottom. (**d**) TEM image of the $TiO_2$ nanowires.
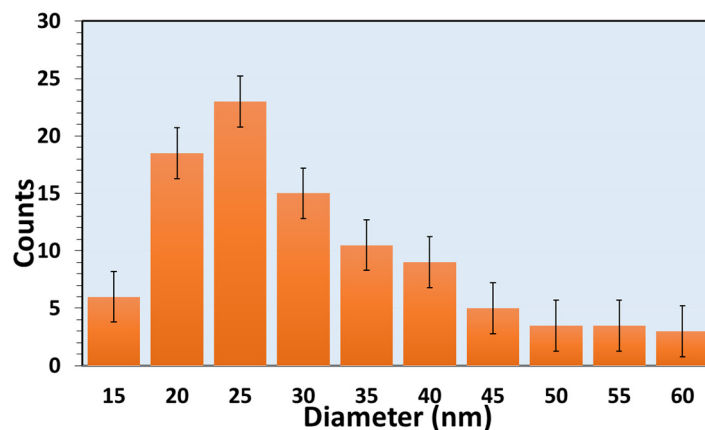
**Figure 3.** Diameter distribution of the thermally oxidized TiO$_2$ nanowires growth at 700 °C with 10 SCCM oxygen and 100 SCCM argon flow for 3 h.

Figure 4 reports the SEM images of Au/Ti samples grown in the presence of 10 SCCM oxygen and 100 SCCM argon flow for 3 h at different temperatures. At 600 °C (Figure 4a), TiO$_2$ grains are well distinguished on the surface but NWs appear only in a few spots with a nonuniform distribution and very short length. A huge difference was observed by increasing the temperature to 650 °C. Figure 4b shows the long and thin NWs grown at this temperature. However, no significant growth improvements can be obtained by increasing the oxidation time to 4 h at 650 °C. In addition, wide grains are observed beneath the NWs. On the contrary, dense, long, and thin NWs were formed when the oxidation temperature was increased to 700 °C (Figure 4c). Early studies demonstrate that the Ti diffusion temperature required to form nanowires is above 800 °C (in Ti foils) [20,32]. Nevertheless, we observed that this temperature decreases to 650 °C in the presence of Au nanoparticles. At 750 °C, instead, thick nanorod-like structures can be observed at the bottom of the NWs, confirming that 700 °C is the optimum temperature for TiO$_2$ NWs growth.
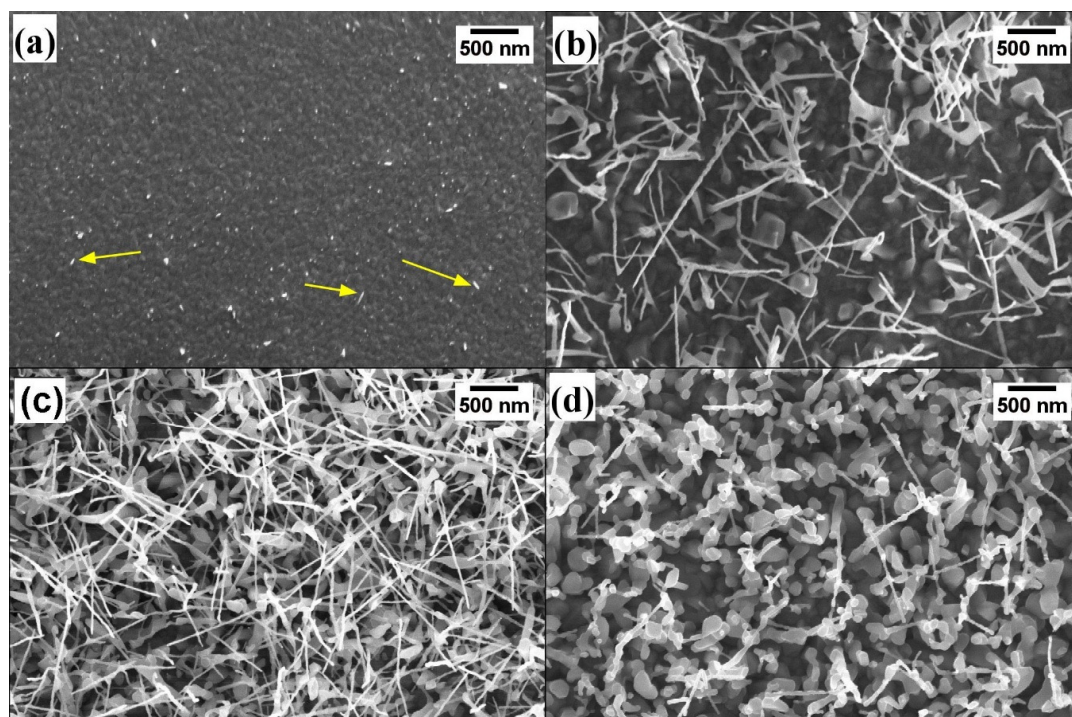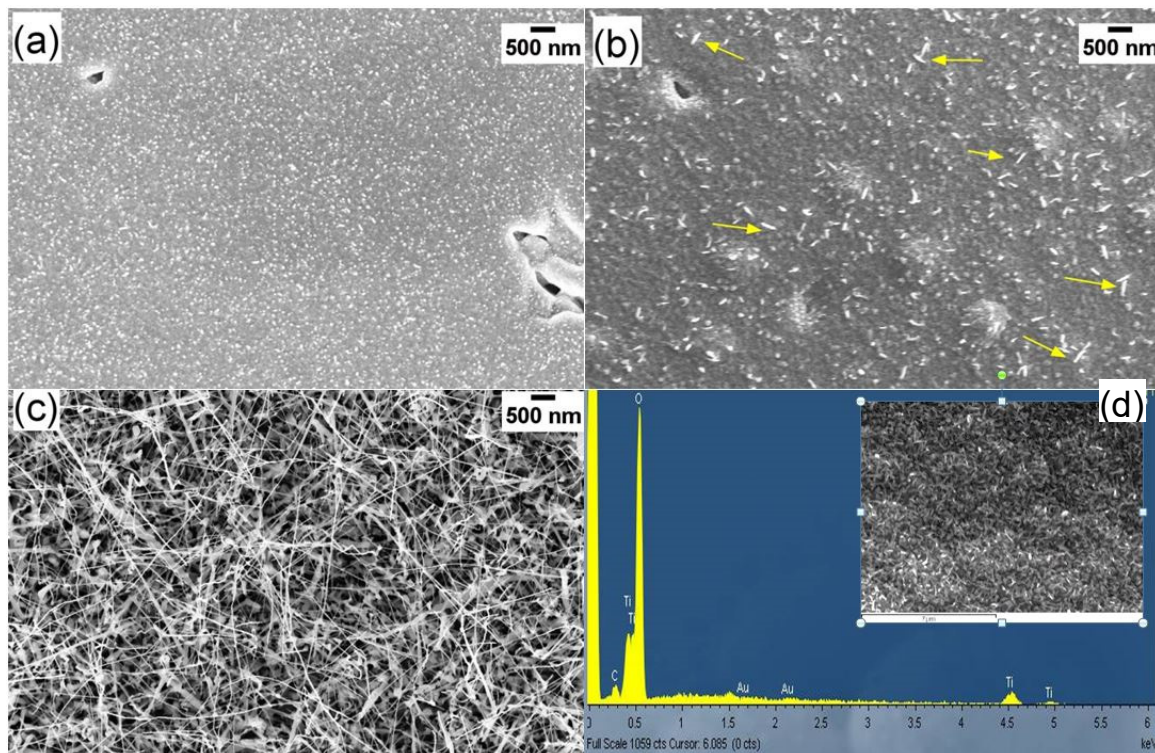


**Figure 4.** SEM view of TiO$_2$ nanowires grown at different temperatures: (**a**) 600, (**b**) 650, (**c**) 700, and (**d**) 750 °C. Oxidation time was 3 h and the oxygen and Ar flow was set 10 and 100 SCCM, respectively.

Figure 5 reports the effect of the layer thickness on the synthesis of $TiO_2$ nanostructures, which is significant. It is not possible to observe any $TiO_2$ NWs if the thickness of the Ti metal layer is 50 nm (Figure 5a). The NWs growth, instead, is well visible on 200 nm thickness films (Figure 5c), while very short and few NWs can be seen when the thickness is decreased to 100 nm (Figure 5b). Figure 5d shows the EDX spectra of thermally oxidized 200 nm film, revealing the presence of Au. In fact, minor Au peaks can be seen at 2.3 KeV, confirming the presence of Au after the oxidation process on the nanowires tip.

No significant changes were observed by varying the oxygen flow from 1 to 20 SCCM. Finally, we studied the effect of oxidation time also. Thin and long NWs were observed when the oxidation time was set to 3 h, and further oxidation results in the growth of flake-like structures. Thanks to the previous considerations, optimum conditions for the synthesis of $TiO_2$ NWs were identified. The optimal Ti layer thickness was 200 nm, the gas flow was 10 SCCM of oxygen and 100 SCCM of argon, 3 h of deposition, and an oxidation temperature of 700 °C.

Apart from the SEM and TEM analysis, $TiO_2$ NWs were also analyzed by Raman spectroscopy (Figure 6), confirming the rutile crystalline structure. $TiO_2$ active vibrations were located at 142 $cm^{-1}$ ($B_{1g}$), 238 $cm^{-1}$ (broad band), and 444 $cm^{-1}$ ($E_g$), 624 $cm^{-1}$ ($A_{1g}$), and 824 $cm^{-1}$ ($B_{2g}$) [36–38]. The broad Raman band at 238 $cm^{-1}$ could be due to the second-order scattering or disorder effects. Galstyan et al. reported the phase transition from anatase to rutile at the annealing temperature of 500 °C [3]. Therefore, our results are in good agreement with the theoretical analysis and published data, confirming that the $TiO_2$ NWs prepared by the proposed method have a rutile phase without any significant impurities [39,40].



**Figure 5.** SEM view of $TiO_2$ nanowires grown from different film thicknesses: (**a**) 50, (**b**) 100, (**c**) 200 nm at 700 °C, (**d**) EDX spectra of the 200 nm thick $TiO_2$ NWs sample. Oxygen flow and Ar flow were set at 10 and 100 SCCM, respectively.
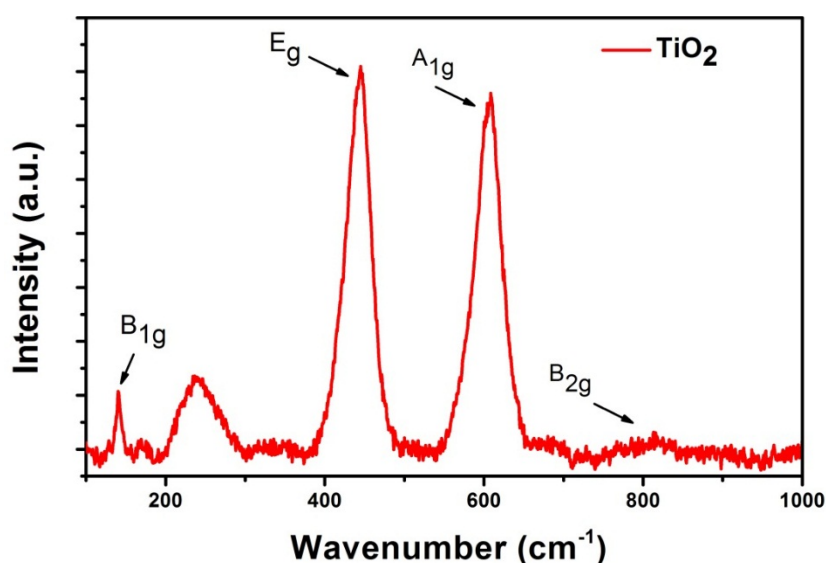
**Figure 6.** Raman spectrum of $TiO_2$ nanowires growth at 700 °C, 10 SCCM oxygen, and 100 SCCM argon flow for 3 h.

### 3.2. Growth Mechanism

SEM, EDX, and TEM images confirmed the presence of Au nanoparticles on the tip of the $TiO_2$ NWs, showing that the process may be similar to the vapor liquid solid (VLS). However, in our case there is no external Ti source: The Ti source is directly the sputtered Ti layer. Ti reacts with oxygen forming a $TiO_2$ film when exposed to an oxygen environment. Then, the oxygen further diffuses through the oxide layer to the metal interface, causing a polycrystalline grain growth (Figure 7). Previous studies have shown that Ti atoms diffuse from the Ti layer to Au, forming intermetallic phases $TiAu_4$, $TiAu_2$, TiAu, and $Ti_3Au$ [41]. The diffusion can occur in a local gradient of chemical potentials in the presence of Au NPs [32,42]. The presence of the Au catalyst is of utmost importance in the synthesis of Ti NWs, as Au promotes preferential nucleation of $TiO_2$ on its surface and it also suppresses $TiO_2$ nucleation on other sites of the substrate. The presence of oxygen in the atmosphere promotes the elongated growth of $TiO_2$ along the principal growth direction. The wider base and the tapering shape of the NWs can be explained based on the diffusion of Ti from the sputtered layer during the growth. This base can be clearly observed when the oxidation time is longer than 3 h. Figure 7 shows that few NWs cause a change of direction with very sharp edges. This is due to the extended defects in the crystallographic structure of the NWs [32]. These defects can lead to an abrupt change of crystal structure orientation in NWs, which results in a sharp change of the main growth direction.
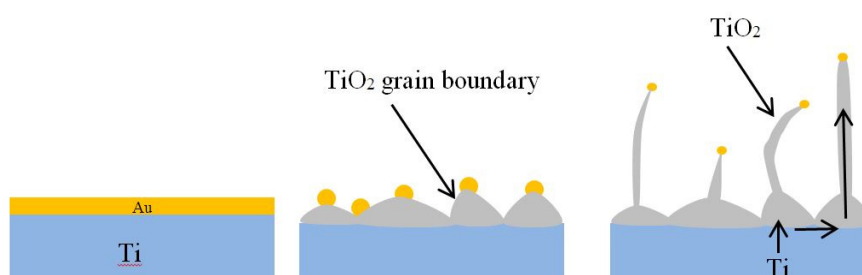


**Figure 7.** Effect of the Au catalyst on the growth of $TiO_2$ NWs.

### 3.3. Gas Sensing

Optimized samples (Ti layer thinness 200 nm, 10 SCCM of oxygen flow, 3 h, and oxidation temperature at 700 °C) were used to fabricate chemical sensing devices and for their characterization in

the presence of target chemical compounds. More specifically, we have investigated the conductometric response of the fabricated material in the presence of different chemical species such as ethanol, acetone, $H_2$, and CO in a wide temperature range (300–500 °C), in order to understand the sensing behavior. Figure 8 shows the dynamic response of $TiO_2$ NWs towards ethanol, acetone, $H_2$, and CO at a working temperature of 400 °C. The electrical conductance increases when introducing a reducing gas and increases with the gas concentration. As the synthetic air flow is restored, the conductance decreases recovering the baseline value. This behavior is typical of n-type semiconductors. At the operating temperature of 300 °C and below, the conductance is very low and noisy. Moreover, the response is very low toward the investigated chemical compounds. Figure 9 reports the short-term stability of the $TiO_2$ NWs based gas sensors, resulting in the exposure of the same gas concentrations over a short period. A very small change in the baseline conductance was observed within the different cycles. On the other hand, the sensor response towards ethanol and hydrogen slightly decreased after the first measurements, probably due to thermal stabilization over the measuring period. The response was stable after the first exposure to the target analyte.
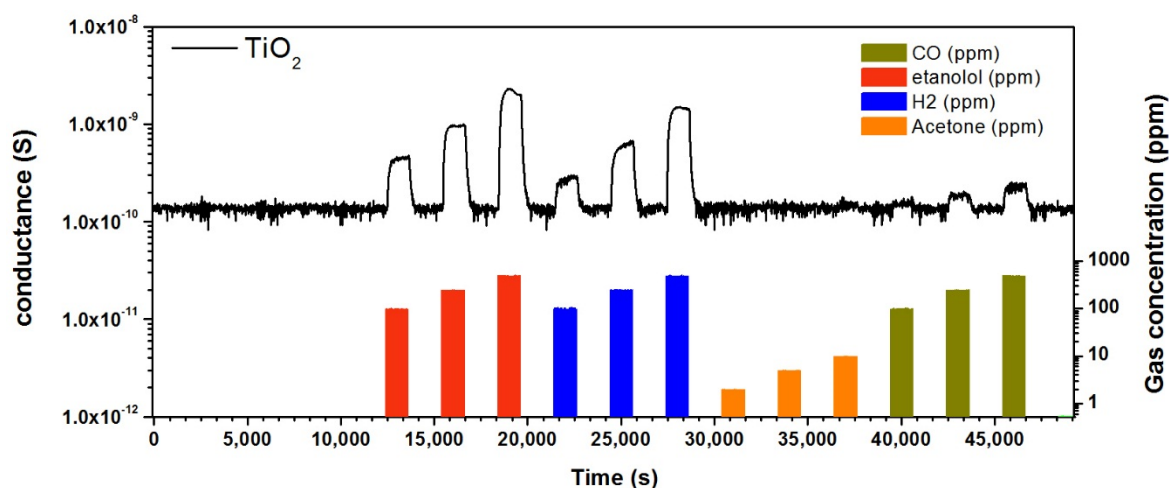


**Figure 8.** Dynamic response of $TiO_2$ NWs toward ethanol (100, 250, 500 ppm), $H_2$ (100, 250, 500 ppm), acetone (2, 5, 10 ppm), and CO (100, 250, 500 ppm) at 400 °C. RH = 40%, with an applied voltage equal to 1 V.
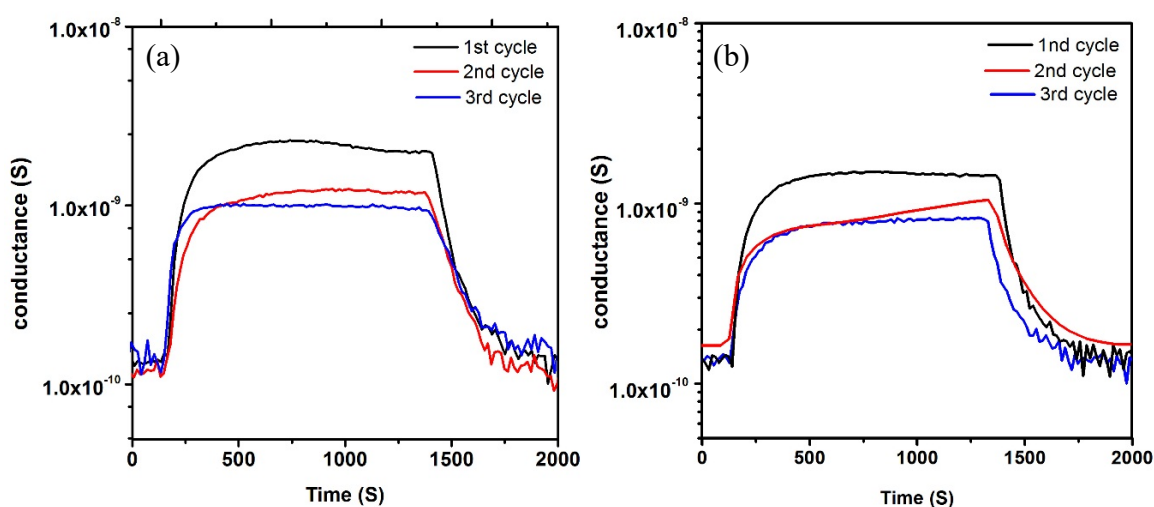


**Figure 9.** The repeatability of $TiO_2$ NWs sensors at 400 °C exposed to (**a**) ethanol (500 ppm) (**b**) hydrogen (500 ppm). RH = 40%, with an applied voltage equal to 1 V.

Figure 10 indicates the temperature dependence of the device performances in terms of response. Overall, $TiO_2$ NWs show good responses to ethanol and $H_2$. The response toward hydrogen is maximum at 400 °C, while it decreases at higher temperatures. The response of $TiO_2$ NWs towards ethanol is high at all working temperatures; nevertheless, also for ethanol detection the optimal working temperature is 400 °C. The temperature has a high impact on the response for ethanol, it increases more than two times from 300 to 400 °C. A low response was observed for CO even at 500 °C, less than one at any operating temperature. We have also tested $TiO_2$ NWs toward other chemical compounds such as acetone, but the response was negligible.
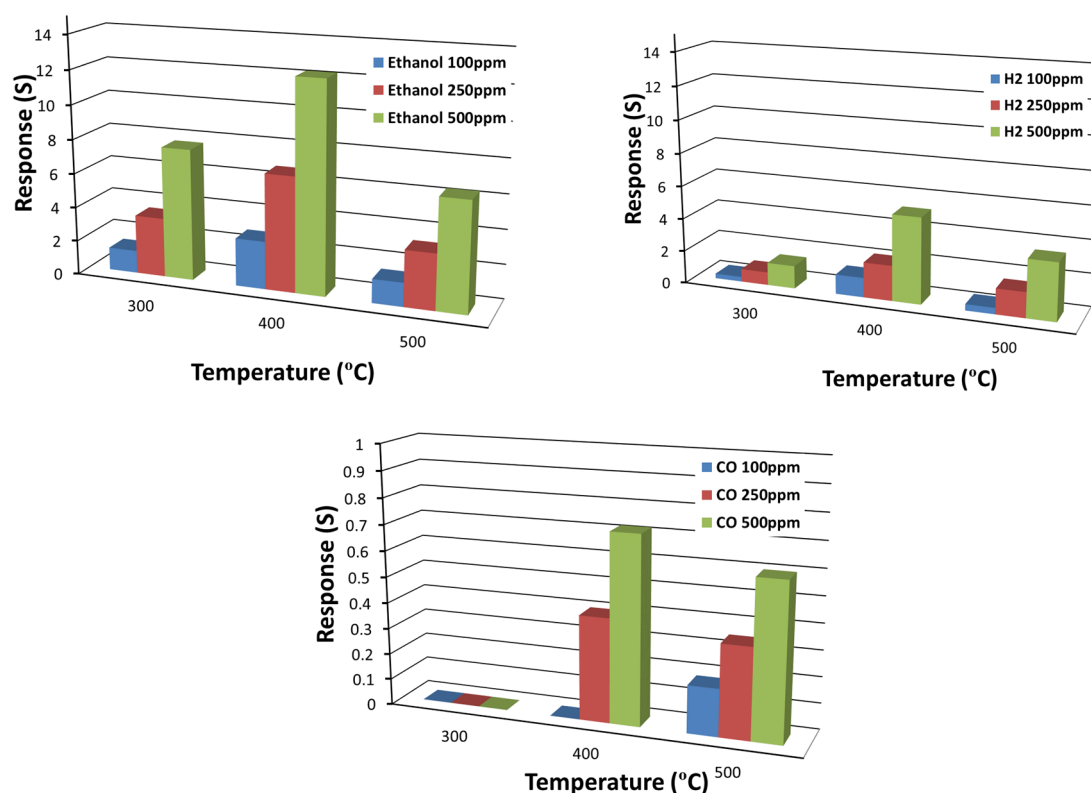
**Figure 10.** Response towards $H_2$, ethanol, and CO in different working temperatures. RH = 40% at 20 °C with applied voltage equal to 1 V.

The response time and recovery time could be defined as the time to reach 90% of the steady state of $G_{gas}$ and $G_{air}$, respectively. Figure 11 shows the influence of the temperature and gas concentrations towards both response time and recovery time. The response time for ethanol is about 2 to 4 min at all temperatures ranging from 300 to 500 °C (Figure 11a). In addition, the response time at 300 °C is lower compared to 500 °C. The recovery time is more than 2 min at 300 °C and less than one minute at 400 °C, indicating that these sensors have a fast recovery. The response time and recovery time is less than 4 min for hydrogen and it decreases for higher working temperatures. Moreover, Figure 11 shows that the gas concentration has no significant impact on the response time and recovery times. Considering the volume of the test chamber (1 L) and the gas flow used (200 SCCM), it takes approximately 15 min to have a complete atmosphere change inside the measuring chamber, by pumping three times the volume of the chamber. Nevertheless, from Figure 11 we may observe that the devices start responding before this complete atmosphere change (<4 min). Therefore, we can suppose that the response and recovery times are overestimated and that the sensing devices are much faster than reported.
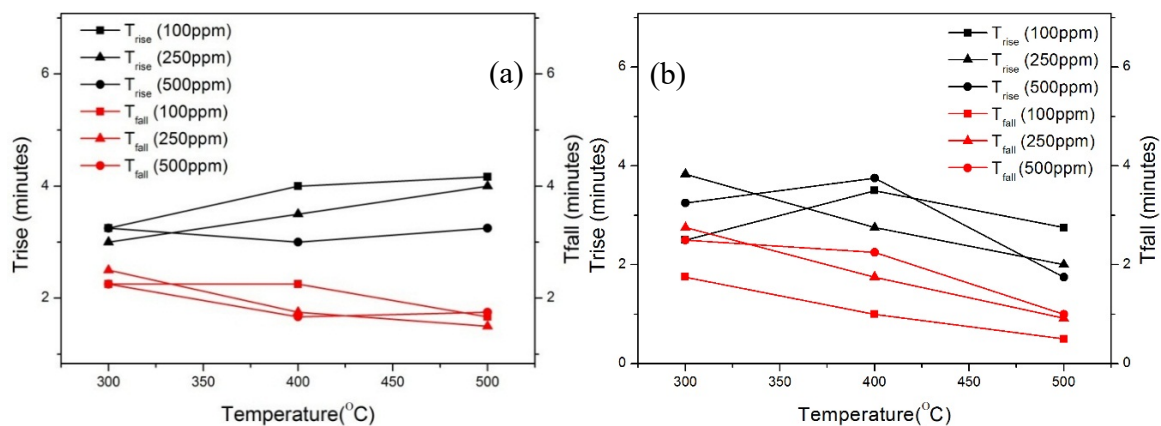
**Figure 11.** Response time and recovery time of the TiO$_2$ NWs in the temperature range of 300–500 °C to (**a**) ethanol (**b**) hydrogen.

Figure 12 shows the estimated calibration curve and power fitting for TiO$_2$ NWs for ethanol and H$_2$ at optimum working temperatures. The experimental data can be fitted by a typical power relation for metal oxide conductometric sensors:

$$\text{Response} = A[\text{Gas concentration}]^B \tag{2}$$

where A and B are constants typical of the gas sensing material and stoichiometry of the involved reactions. The detection limit was calculated by taking one as a threshold response to ethanol and H$_2$. These TiO$_2$ NW detection limits for ethanol and H$_2$ were identified as 30 and 90 ppm, respectively. The detection limit for ethanol is lower compared to H$_2$. Table 2 summarizes the values of A and B coefficients and the detection limits of TiO$_2$ NWs.
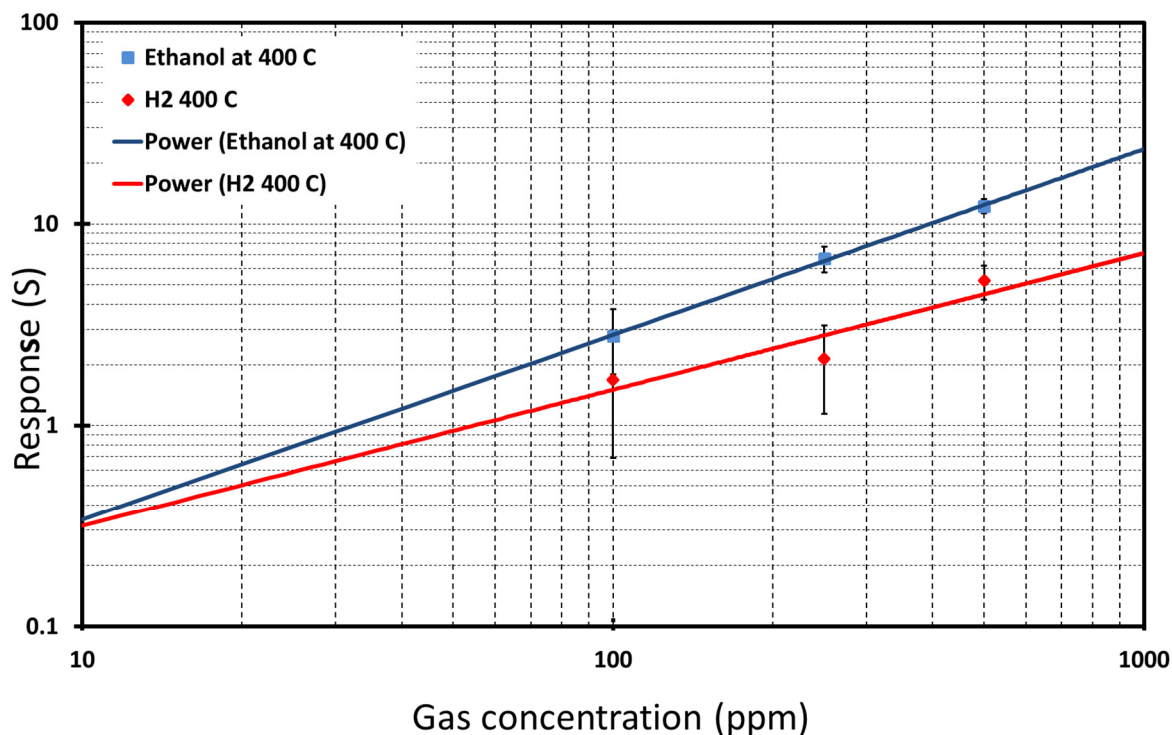


**Figure 12.** Calibration curves of TiO$_2$ NWs reporting the response versus gas concentration at optimal temperatures and relative humidity of 40% at 20 °C.

Table 3 reports the literature data on gas sensing properties of TiO$_2$ NWs and nanobelts, synthesized by various methods, towards ethanol and hydrogen. TiO$_2$ nanobelts and nanowires synthetized via the hydrothermal technique exhibit good responses to ethanol at 350–400 °C in the presence of humidity [43,44]. However, most of the other results show a good response only in the absence of humidity [45–47]. Moreover, as a hydrogen gas sensing material, it shows a noble response to 500 PPM at 400 °C by comparing with other results [48,49]. However, most of the studies have been carried out in a high concentration of hydrogen or without the humidity environment [50–52]. From these results, it can be concluded that TiO$_2$ NWs grown by thermal oxidation show a high response to ethanol and H$_2$ even compared to state-of-the-art results.

**Table 2.** Power law calibration coefficients and detection limits of TiO$_2$ for ethanol and H$_2$ at optimal working temperatures of 400 °C.

| Gas | Detection Limit (ppm) | A | B |
|---|---|---|---|
| Ethanol | 32 | 0.0405 | 0.9214 |
| H$_2$ | 90 | 0.0173 | 0.9029 |

**Table 3.** Summary of H$_2$ and ethanol sensing performances of TiO$_2$ NWs.

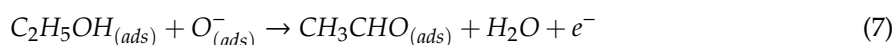| Synthesis Method | Composition | Gas | Gas Con: (ppm) | Temp: (°C) | RH% | Res (S) | Ref |
|---|---|---|---|---|---|---|---|
| Hydrothermal | Nano belts | | 400 | 350 | 40 | 13 | [43] |
| Hydrothermal | Nanowires | | 1000 | 500 | 30 | 4.5 | [44] |
| Electrospinning | Nanowires | Ethanol | 1000 | 400 | 0 | 15.8 | [45] |
| Hydrothermal | Nanowires | | 500 | 400 | 0 | 6 | [46] |
| Hydrothermal | Nanotubes | | 47 | 500 | 0 | 15 | [47] |
| Thermal oxidation | Nanowires | | 500 | 400 | 40 | 15 | This work |
| VLS | Nanowires | | 1000 | 500 | 0 | 1 | [48] |
| Hydrothermal | Nanotubes | | 500 | 500 | 0 | 9.6 | [47] |
| Anodic oxidation | Nanotubes | | 100 | 150 | 0 | 18 | [49] |
| Hydrothermal | Nanorods | Hydrogen | 1000 | 200 | 0 | 0.87 | [50] |
| Electrochemical Anodization | Nanotubes | | 20,000 | 25 | 0 | 0.25 | [51] |
| Hydrothermal | Nanowires | | 5 | RT | 0 | 3.5 | [52] |
| Thermal oxidation | Nanowires | | 500 | 400 | 40 | 5.2 | This work |

### 3.4. Gas Sensing Mechanism

The sensing properties of the TiO$_2$ NWs are based on the change of the electrical resistance due to the adsorption and desorption of the chemical species from the surface of the sensing material. This mechanism has been adopted for many semiconductor metal oxides and it was described elsewhere in detail [53]. When the sensor is exposed to air, oxygen molecules adsorb on the TiO$_2$ surface, forming oxygen ions, and capturing electrons from its conduction band, leading to an increase of the metal oxide electrical resistance. The reaction kinetics are shown by the following reactions [54]:

$$O_{2(gas)} \rightarrow O_{2(ads)} \tag{3}$$

$$O_{2(ads)} + e \rightarrow O^-_{2(ads)} \tag{4}$$

$$O^-_{2(ads)} + e \rightarrow 2O^-_{(ads)} \tag{5}$$

$$O^-_2 + e \rightarrow O^{2-}_{(ads)} \tag{6}$$

Some oxygen atoms may diffuse and spill over from the Au nanoparticles onto TiO$_2$ NWs, capturing electrons from the conduction band. This mechanism increases oxygen adsorption, resulting in an enhancement of NWs interaction with the target gas molecules. When the sensors are exposed to ethanol and H$_2$, gas molecules may be chemisorbed and react with adsorbed oxygen

species to form $H_2O$. This will result in the release of trapped electrons back to $TiO_2$ with a decrease in the sensor resistance. Possible reactions are as follows:

$$C_2H_5OH_{(ads)} + O^-_{(ads)} \rightarrow CH_3CHO_{(ads)} + H_2O + e^- \tag{7}$$

$$H_2 + O^-_{(ads)} \rightarrow H_2O_{(gas)} + e^- \tag{8}$$

## 4. Conclusions

In conclusion, $TiO_2$ NWs were grown on the alumina substrate by the seed assisted thermal oxidation method. RF magnetron sputtering was used to deposit Ti and Au layers. Thermal oxidation was carried out in an oxygen deficient environment. Morphological characterization revealed the presence of Au nanoparticles on top of the NWs, indicating that the Au catalyst drove the growth process. Raman spectroscopy confirmed the rutile crystalline phase of the material. All the morphological investigations confirmed that the oxidation temperature, film thickness, and oxidation time play a crucial role in the growth of $TiO_2$ NWs. Moreover, gas sensing measurements showed the ability of $TiO_2$ NWs to detect ethanol and $H_2$ at an optimal temperature of 400 °C. The detection limits resulted below 50 and 100 ppm for ethanol and $H_2$, respectively. These results demonstrate that $TiO_2$ NWs are good candidates for the fabrication of a chemical/gas sensing device. Moreover, this synthesis technique may be adopted further to grow $TiO_2$ NWs on different transducers for their employment in applications such as photo electrochemical water spitting and solar cells.

**Author Contributions:** Conceptualization, H.M.M.M.A., D.Z. and E.C.; methodology, D.Z.; validation, H.M.M.M.A., N.P. and N.H.A.; formal analysis, H.M.M.M.A. and N.G.; investigation, H.M.M.M.A.; resources, H.M.M.M.A. and N.H.A.; data curation, H.M.M.M.A.; writing—original draft preparation, H.M.M.M.A. and N.G.; writing—review and editing, E.C.; visualization, H.M.M.M.A.; supervision, E.C.; project administration, E.C.; funding acquisition, N.G., D.Z. and E.C. All authors have read and agreed to the published version of the manuscript.

**Conflicts of Interest:** The authors declare no conflict of interest.

## References

1. Gerasimov, G.N.; Gromov, V.F.; Ilegbusi, V.F.; Trakhtenberg, L.I. The mechanisms of sensory phenomena in binary metal oxide nanocomposites. *Sens. Actuators B Chem.* **2017**, *240*, 613–624. [CrossRef]
2. Wang, C.; Yin, L.; Zhang, L.; Xiang, D.; Gao, R. Metal Oxide Gas Sensors: Sensitivity and Influencing Factors. *Sensors* **2010**, *10*, 2088–2106. [CrossRef] [PubMed]
3. Rahman, M.A.; Bazargan, S.; Srivastava, S.; Wang, X.; Ellah, M.A.; Thomas, J.P.; Heinig, N.F.; Pradhan, D.; Leung, K.T. Defect-rich decorated $TiO_2$ nanowires for super-efficient photoelectrochemical water splitting driven by visible light. *Energy Environ. Sci.* **2015**, *8*, 3363–3373. [CrossRef]
4. Park, N.G.; Lagemaat, J.V.D.; Frank, A.J. Comparison of Dye-Sensitized Rutile- and Anatase-Based $TiO_2$ Solar Cells. *J. Phys. Chem. B* **2000**, *104*, 8989–8994. [CrossRef]
5. Appell, D. Wired for success. *Nature* **2002**, *419*, 553–555. [CrossRef]
6. Ni, M.; Leung, M.K.; Leung, D.Y.; Sumathy, K. A review and recent developments in photocatalytic water-splitting using $TiO_2$ for hydrogen production. *Renew. Sustain. Energy Rev.* **2007**, *11*, 401–425. [CrossRef]

7.　　Galstyana, V.; Comini, E.; Baratto, C.; Mazhar, M.E.; Ponzoni, A.; Sberveglieri, V.; Poli, N.; Faglia, G.; Sberveglieri, G. Conductance and work function of $TiO_2$ nanotubes based gas sensors. *Procedia Eng.* **2005**, *120*, 769–772. [CrossRef]

8.　　Galstyan, V. Porous $TiO_2$-based gas sensors for cyber chemical systems to provide security and medical diagnosis. *Sensors* **2017**, *17*, 12. [CrossRef]

9.　　Galstyan, V.; Ponzoni, A.; Kholmanov, I.; Comini, E.; Sberveglieri, V.; Poli, N.; Sberveglieri, G. Hierarchically Assembled Titania Based Nanostructures: Innovative and Efficient Strategies for the Synthesis and the Improvement of Sensing. *MDPI Proc.* **2017**, *1*, 293. [CrossRef]

10.　Kwoka, M.; Galstyan, V.; Comini, E.; Szuber, J. Pure and highly Nb-doped titanium dioxide nanotubular arrays: Characterization of local surface properties. *Nanomaterials* **2007**, *7*, 456. [CrossRef]

11.　Lee, S.H.; Galstyan, V.; Ponzoni, A.; Juan, I.G.; Riedel, R.; Dourges, M.A.; Nicolas, Y.; Toupance, T. Finely Tuned $SnO_2$ Nanoparticles for Efficient Detection of Reducing and Oxidizing Gases: The Influence of Alkali Metal Cation on Gas-Sensing Properties. *ACS Appl. Mater. Interfaces* **2018**, *10*, 10173–10184. [CrossRef] [PubMed]

12.　Epifani, M.; Andreu, T.; Zamani, R.; Arbiol, J.; Comini, E.; Siciliano, P.; Fagli, G.; Morante, J.R. Pt doping triggers growth of $TiO_2$ nanorods: Nanocomposite synthesis and gas-sensing properties. *CrystEngComm* **2012**, *14*, 3882–3887. [CrossRef]

13.　Lee, J.C.; Park, K.S.; Kim, T.G.; Choi, H.J.; Sung, Y.M. Controlled growth of high-quality $TiO_2$ nanowires on sapphire and silica. *Nanotechnology* **2006**, *17*, 4317–4321. [CrossRef]

14.　Park, Y.S.; Lee, J.S. Morphology Control of Single Crystalline Rutile $TiO_2$ Nanowires. *Bull. Korean Chem. Soc.* **2011**, *32*, 3571–3574. [CrossRef]

15.　DSani, S.R.; Ali, A.M.; Jafari, R. The effect of carrier gas flow on structural and optical properties of $TiO_2$ nanowires. *Phys. E Low-Dimens. Syst. Nanostruct.* **2011**, *43*, 1809–1812. [CrossRef]

16.　Pishekloo1, S.P.; Dariani, R.S. Growing $TiO_2$ nanowires by solid–liquid–solid mechanism including two factors (Ti and O). *Appl. Phys. A* **2016**, *122*, 1–10. [CrossRef]

17.　Peng, X.; Wang, J.; Thomas, D.F.; Chen, A. Tunable growth of $TiO_2$ nanostructures on Ti substrates. *Nanotechnology* **2005**, *16*, 2389–2395. [CrossRef]

18.　Peng, X.; Chen, A. Dense high-hydrophobic rutile $TiO_2$ nanorod arrays. *Appl. Phys. A Mater. Sci. Process.* **2005**, *80*, 473–476. [CrossRef]

19.　Huo, K.; Zhang, X.; Hu, L.; Sun, X.; Fu, J.; Chu, P.K. One-step growth and field emission properties of quasialigned $TiO_2$ nanowire/carbon nanocone core-shell nanostructure arrays on Ti substrates. *Appl. Phys. Lett.* **2008**, *93*, 013105. [CrossRef]

20.　Lee, G.H. Synthesis of $TiO_2$ nanowires via thermal oxidation process in air. *Mater. Res. Innov.* **2016**, *20*, 421–424. [CrossRef]

21.　Poudel, B.; Wang, W.Z.; Dames, C.; Huang, J.Y.; Kunwar, S.; Wang, D.Z.; Banerjee, D.; Chen, G.; Ren, Z.F. Formation of crystallized titania nanotubes and their transformation into nanowires. *Nanotechnology* **2005**, *16*, 1935–1940. [CrossRef]

22.　Bhowmik, B.; Dutta, K.; Banerjee, N.; Hazra, A.; Bhattacharyya, P. Low temperature acetone sensor based on Sol-gel grown nano $TiO_2$ thin film. In Proceedings of the 2013 IEEE International Conference ON Emerging Trends in Computing, Communication and Nanotechnology (ICECCN), Tirunelveli, India, 25–26 March 2013; pp. 553–557. [CrossRef]

23.　Losilla, J.A.; Ratanatawanate, C.; Balkus, K.J., Jr. Synthesis of $TiO_2$ nanotube films via pulsed laser deposition followed by a hydrothermal treatment. *J. Exp. Nanosci.* **2014**, *9*, 126–137. [CrossRef]

24.　Nikfarjam, A.; Hosseini, S.; Salehifar, N. Fabrication of a Highly Sensitive Single Aligned $TiO_2$ and Gold Nanoparticle Embedded $TiO_2$ Nano-Fiber Gas Sensor. *ACS Appl. Mater. Interfaces* **2017**, *9*, 15662–15671. [CrossRef] [PubMed]

25.　Shen, J.; Vincent, P.; Blanchard, N.P.; Nicolle, J.; Chouei, M.; Purcell, S.T.; Poncharal, P.; Salles, V.; Brioude, A. Physical properties of individual anatase $TiO_2$ nanowires investigated by field emission in a transmission electron microscope. *J. Vac. Sci. Technol.* **2014**, *30*, 11801. [CrossRef]

26.　Kim, I.D.; Rothschild, A.; Lee, B.H.; Kim, D.Y.; Jo, S.M.; Tuller, H.L. Ultrasensitive Chemiresistors Based on Electrospun $TiO_2$ Nanofibers. *Nano Lett.* **2016**, *6*, 2006–2013. [CrossRef]

27.　Yang, B.Y.; Qu, L.; Dai, L.; Kang, T.; Durstock, M. Electrophoresis Coating of Titanium Dioxide on Aligned Carbon Nanotubes for Controlled Syntheses of Photoelectronic Nanomaterials. *Adv. Mater.* **2007**, *19*, 1239–1243. [CrossRef]

28. Wang, J.; Lin, Z. Anodic formation of ordered TiO$_2$ nanotube arrays: Effects of electrolyte temperature and anodization potential. *J. Phys. Chem. C* **2009**, *113*, 4026–4030. [CrossRef]

29. Mortezaali, A.; Sani, S.R. Study of growth parameters on structural properties of TiO$_2$ nanowires. *J. Nanostruct. Chem.* **2013**, *3*, 1–6. [CrossRef]

30. Dariani, R.S.; Qaleh, Z.N. Microstructure characterization of TiO$_2$ nanowires fabricated by thermal evaporation process. *Thin Solid Film.* **2013**, *542*, 192–198. [CrossRef]

31. Shang, Z.G.; Liu, Z.Q.; Shan, P.J.; Shang, J.K. Synthesis of Single-Crystal TiO$_2$ Nanowire Using Titanium Monoxide Powder by Thermal Evaporation. *J. Mater. Sci. Technol.* **2012**, *28*, 385–390. [CrossRef]

32. Arcadipane, E.; Sanz, R.; Amiard, G.; Boninelli, S.; Impellizzeri, G.; Privitera, V.; Bonkerud, J.; Bhoodoo, C.; Vines, L.; Svenssonc, B.G.; et al. Single-crystal TiO$_2$ nanowires by seed assisted thermal oxidation of Ti foil: Synthesis and photocatalytic properties. *RSC Adv.* **2017**, *7*, 11222. [CrossRef]

33. Lee, H.; Dregia, S.; Akbar, S.; Alhoshan, M. Growth of 1-D TiO$_2$ Nanowires on Ti and Ti Alloys by Oxidation. *J. Nanomater.* **2010**, *2010*, 503186. [CrossRef]

34. Peng, X.; Chen, A. Aligned TiO$_2$ nanorod arrays synthesized by oxidizing titanium with acetone. *J. Mater. Chem.* **2004**, *14*, 2542–2548. [CrossRef]

35. Kolasinski, K.W. Catalytic growth of nanowires: Vapor–liquid–solid, vapor–solid–solid, solution–liquid–solid and solid–liquid–solid growth. *Curr. Opin. Solid State Mater. Sci.* **2007**, *10*, 182–191. [CrossRef]

36. Galstyan, V.; Comini, E.; Baratto, C.; Ponzoni, A.; Ferroni, M.; Poli, N.; Bontempi, E.; Brisotto, M.; Faglia, G.; Sberveglieri, G. Large surface area biphase titania for chemical sensing. *Sens. Actuators B Chem.* **2015**, *209*, 1091–1096. [CrossRef]

37. Gao, T.; Fjellvåg, H.; Norby, P. Crystal structures of titanate nanotubes: A Raman scattering study. *Inorg. Chem.* **2009**, *48*, 1423–1432. [CrossRef] [PubMed]

38. Gao, T.; Fjellvåg, H.; Norby, P. Raman scattering properties of a protonic titanate H$_x$Ti$_{2-x/4}$[]$_{x/4}$O$_4$.H$_2$O ([], vacancy; x = 0.7) with lepidocrocite-type layered structure. *J. Phys. Chem. B* **2008**, *112*, 9400–9405. [CrossRef]

39. Frank, O.; Zukalova, M.; Laskova, B.; Kürti, J.; Koltai, J.; Kavan, L. Raman spectra of titanium dioxide (anatase, rutile) with identified oxygen isotopes. *Phys. Chem. Chem. Phys.* **2012**, *14*, 14567–14572. [CrossRef]

40. Lubas, M.; Jasinski, J.J.; Sitarz, M.; Kurpaska, L.; Podsiad, P.; Jasinski, J. Raman spectroscopy of TiO$_2$ thin films formed by hybrid treatment for biomedical applications. *Spectrochimica. Acta-Part A Mol. Biomol. Spectrosc.* **2014**, *133*, 867–871. [CrossRef]

41. Martinez, W.E.; Gregori, G.; Mates, T. Titanium diffusion in gold thin films. *Thin Solid Film.* **2010**, *518*, 2585–2591. [CrossRef]

42. Sylwestrowicz, W.D.; Elkholy, H.A.; Kammlott, G.W. The effect of temperature and humidity on interdiffusion of gold and titanium in thin films. *J. Mater. Sci.* **1979**, *14*, 873–881. [CrossRef]

43. Zeng, W.; Lui, T.; Wang, Z. Enhanced gas sensing properties by SnO$_2$ nanosphere functionalized TiO$_2$ nanobelts. *J. Mater. Chem.* **2012**, *22*, 3544–3548. [CrossRef]

44. Zhou, Y.; Ding, Q.; Li, J.; Wang, Y.; Wang, B.; Zhu, W.; AoOuyang, X.; Liu, L.; Wang, Y. Enhanced sensing performance of TiO$_2$/Ag$_2$V$_4$O$_{11}$ nanoheterostructures to ethanol gas. *J. Alloys Compd.* **2019**, *811*, 151958. [CrossRef]

45. Zhou, M.; Liu, Y.; Wu, Y.; Zhang, X. Different crystalline phases of aligned TiO$_2$ nanowires and their ethanol gas sensing properties. *Phys. E Low-Dimens. Syst. Nanostruct.* **2019**, *114*, 113601. [CrossRef]

46. Deng, J.; Yo, B.; Lou, Z.; Wang, L.; Wang, R.; Zhang, T. Facile synthesis and enhanced ethanol sensing properties of the brush-like ZnO–TiO$_2$ heterojunctions nanofibers. *Sens. Actuators B Chem.* **2013**, *184*, 21–26. [CrossRef]

47. Seo, M.H.; Yuasa, M.; Kida, T.; Huh, J.S.; Shimanoe, K.; Yamazoe, N. Gas sensing characteristics and porosity control of nanosturctured films composed of TiO$_2$ nanotubes. *Sens. Actuators B Chem.* **2009**, *137*, 513–520. [CrossRef]

48. Meng, D.; Yamazaki, T.; Kikuta, T. Preparation and gas sensing properties of undoped and Pd-doped TiO$_2$ nanowires. *Sens. Actuators B Chem.* **2014**, *190*, 838–843. [CrossRef]

49. Sennik, E.; Colak, Z.; Kilic, N.; Ozturk, Z.Z. Sytnhesis of hughly-orderd TiO2 nanotubes for a hydrigen sensor. *Int. J. Hydrog. Energy* **2010**, *35*, 4420–4427. [CrossRef]

50. Sennik, E.; Alev, O.; Ozturk, Z.Z. The effect of Pd on the H$_2$ and VOC sensing properties of TiO$_2$ nanorods. *Sens. Actuators B Chem.* **2016**, *229*, 692–700. [CrossRef]

51.  Li, Z.; Ding, D.; Liu, Q.; Wang, Z. Ni-doped TiO$_2$ nanotubes for wide-range hydrogen sensing. *Nanoscale Res. Lett.* **2014**, *9*, 118. [CrossRef]

52.  Ren, S.; Liu, W. One-step photochemical deposition of PdAu alloyed nanoparticles on TiO$_2$ nanowires for ultra-sensitive H$_2$ detection. *J. Mater. Chem. A* **2016**, *4*, 2236–2245. [CrossRef]

53.  Bertuna, A.; Faglia, G.; Ferroni, M.; Kaur, N.; Munasinghe, H.M.M.M.; Sberveglieri, G.; Comini, E. Metal oxide nanowire preparation and their integration into chemical sensing devices at the SENSOR lab in Brescia. *Sensors* **2017**, *17*, 1000. [CrossRef]

54.  Munasinghe, M.A.H.M.; Zappa, D.; Poli, N.; Gunawardhana, N.; Comini, E. Gold functionalized MoO$_3$ nano flakes for gas sensing applications. *Sens. Actuators B Chem.* **2018**, *269*, 331–339. [CrossRef]